HHS Public Access

Author manuscript

Dev Neurobiol. Author manuscript; available in PMC 2020 May 11.

Published in final edited form as:

Dev Neurobiol. 2019 April ; 79(4): 335–349. doi:10.1002/dneu.22681.

Tao negatively regulates BMP signaling during neuromuscular junction development in *Drosophila*

Stephen F. Politano[1,3,*], **Ryan R. Salemme**[1,4,*], **James Ashley**[2,*], **Javier A. Lopez-Rivera**[1,5], **Toren A. Bakula**[1], **Kathryn A. Puhalla**[1], **John P. Quinn**[1], **Madison J. Juszczak**[1], **Lauren K. Phillip**[1], **Robert A. Carrillo**[2], **Pamela J. Vanderzalm**[1]

[1]Department of Biology, John Carroll University, University Heights, OH, 44118 USA

[2]Molecular Genetics and Cell Biology, University of Chicago, Chicago, IL 60637 USA

[3]Present address: The Ohio State University College of Medicine, Columbus, OH, 43210 USA

[4]Present address: State University of New York at Buffalo Jacobs School of Medicine and Biomedical Sciences, Buffalo, NY, 14260 USA

[5]Present address: Program in Molecular Medicine, Cleveland Clinic Lerner Research Institute, Cleveland, OH, 44195 USA

Abstract

The coordinated growth and development of synapses is critical for all aspects of neural circuit function and mutations that disrupt these processes can result in various neurological defects. Several anterograde and retrograde signaling pathways, including the canonical Bone Morphogenic Protein (BMP) pathway, regulate synaptic development in vertebrates and invertebrates. At the *Drosophila* larval neuromuscular junction (NMJ), the retrograde BMP pathway is part of the machinery that controls NMJ expansion concurrent with larval growth. We sought to determine whether the conserved Hippo pathway, critical for proportional growth in other tissues, also functions in NMJ development. We found that neuronal loss of the serine-threonine protein kinase Tao, a regulator of the Hippo signaling pathway, results in supernumerary boutons, each of which contain a normal number of active zones. *Tao* is also required for proper synaptic function, as reduction of *Tao* results in NMJs with decreased evoked excitatory junctional potentials. Surprisingly, *Tao* function in NMJ growth is independent of the Hippo pathway. Instead, our experiments suggest that *Tao* negatively regulates BMP signaling as reduction of *Tao* leads to an increase in pMad levels in motor neuron nuclei and an increase in BMP target gene expression. Taken together, these results support a role for *Tao* as a novel inhibitor of BMP signaling in motor neurons during synaptic development and function.

Keywords

Tao; NMJ development; BMP signaling; Hippo signaling

Corresponding author: pvanderzalm@jcu.edu.

*These authors contributed equally to this work

Data Availability Statement: The data that support the findings of this study are available from the corresponding author upon reasonable request.

Introduction

The larval neuromuscular junction (NMJ) of *Drosophila melanogaster* is a glutamatergic synapse used as a model system for AMPA/kainate synapses of the vertebrate central nervous system (CNS). The basic muscle and innervation architecture is established embryonically, with axon growth cones arriving at their target muscle(s) and transitioning into synaptic terminals containing structures called boutons before hatching (Keshishian et al., 1993; Menon et al., 2013; Yoshihara et al., 1997). Boutons contain multiple discrete active zones, the actual sites where neurotransmitter-containing vesicles accumulate for release, and are opposed by clusters of glutamate receptors on the postsynaptic muscle. One of the challenges during larval development is the incredibly rapid growth period that follows hatching. The larval body wall muscle area will increase 100-fold over the next four days, and the motor neuron connections that innervate these muscles must grow in concert (Guan et al., 1996; Keshishian & Chiba, 1993). This growth comes in the form of more boutons and active zones to maintain synaptic efficacy (Gorczyca et al., 1993; Menon et al., 2013; Ruiz-Canada & Budnik, 2006). Though the morphology of each NMJ at the end of larval development is unique, a stereotypical number of boutons are formed at each muscle. Similarly, each NMJ arbor contains a stereotypical number of active zones.

Some of the evolutionarily conserved signaling pathways regulating this remarkable fidelity of connectivity are well-known, with a non-canonical Wnt pathway mediating anterograde signaling from neuron to muscle, and a canonical BMP signaling pathway mediating retrograde signaling (reviewed in Deshpande & Rodal, 2016; Koles & Budnik, 2012). The BMP pathway at the NMJ utilizes the muscle-derived ligand Glass bottom boat (Gbb) binding to the presynaptic type II receptor Wishful thinking (Wit) together with either Saxophone (Sax) or Thickveins (Tkv) as the type I co-receptor. Activation of the heterotetrameric receptor complex results in trafficking of the receptor complex to the cell soma, where it can phosphorylate and activate the downstream effector Smad (Mad in *Drosophila*) (Smith et al., 2012). Phosphorylated Mad (pMad) then associates with its co-Smad Medea and acts as a transcription factor complex to modify gene expression required for NMJ growth (reviewed in Collins & DiAntonio, 2007; Deshpande & Rodal, 2016). Loss of these core BMP pathway components results in dramatic undergrowth of NMJs (Aberle et al., 2002; Marqués et al., 2002; McCabe et al., 2004; 2003; Rawson et al., 2003). However, some bouton growth is observed when disrupting BMP signaling, suggesting potential crosstalk with other signaling pathways.

A prime candidate for helping establish the coordinated growth between neurons and muscle during synaptic development is the conserved Hippo tumor suppressor pathway, which works to maintain proportional growth in a variety of different tissues, including many epithelia and stem cell populations (Halder & Johnson, 2011; X. Huang et al., 2014; Poon et al., 2016). The core of the pathway consists of three serine/threonine kinases, Tao, Hippo, and Warts, that activate one another sequentially to inhibit the growth-promoting transcriptional co-activator Yorkie (Boggiano et al., 2011; Dong et al., 2007; Poon et al., 2011). Though Hippo signaling has been predominantly described in mitotic tissues, it has also been implicated in post-mitotic developmental processes, such as dendritic arbor tiling

and photoreceptor cell-fate specification (Emoto et al., 2006; Jukam et al., 2013). In addition, Hippo signaling interacts with other conserved signaling pathways, including the BMP pathway. Yorkie can bind to Mad and regulate target gene recognition in Drosophila wing discs (Oh & Irvine, 2011) while Yorkie's vertebrate homolog TAZ can control nuclear localization and activity of Smad/co-Smad complexes in human embryonic stem cells (Varelas et al., 2008). Finally, Tao is robustly expressed in the *Drosophila* embryonic CNS in a pattern reminiscent of the monoclonal antibody BP102, which highlights the axonal tracts of the developing CNS (Pflanz et al., 2015). This raises the possibility that the Hippo pathway, critical for growth control in many contexts, might also be playing a role during BMP-dependent larval NMJ development.

We used a combination of genetic and functional experiments to determine if the Hippo pathway is required for larval NMJ growth. Targeted RNAi for components of the Hippo pathway identified *Tao* as a mediator of bouton expansion. Surprisingly, knockdown of other Hippo pathway components had no impact on NMJ growth. *Tao* is also required for normal NMJ function. In support of a Hippo pathway-independent function, *Tao* was found to be a negative regulator of the BMP pathway. Thus, we identify a novel role for *Tao* in larval NMJ development which is dependent on BMP and not Hippo signaling.

Materials and Methods

Genetics

The following *Drosophila melanogaster* strains were used: *Oregon-R* (Bloomington Drosophila Stock Center, BDSC) w^{1118} (used as a wild-type control, BDSC), *UAS-dcr2; D42-GAL4* (BDSC), *24B-GAL4* (BDSC), *OK6-GAL4* (BDSC), *BG57-GAL4* (Budnik et al., 1996), Tao^{16}*/FM7, dfd-YFP* (Pflanz et al., 2015), independent lines of *UAS-flag-Tao* (lines 8, 61, and 89) and *UAS-flag-*$Tao^{Kinase\text{-}Dead}$ (Boggiano et al., 2011), *UAS-Hpo* (Wu et al., 2003), *UAS-Myc-wts/CyO, dfd-YFP* (Jia et al., 2003), *UAS-flag-Yki* (Xu et al., 2018), *UAS-Tao RNAi-1* (VDRC lines 107645 and 17432 combined in one stock), *UAS-Tao RNAi-2* (Transgenic RNAi Project (TRiP) line HMS01226), *UAS-Tao RNAi-3* (Vienna Drosophila Stock Center (VDRC) line 17432), *UAS-Tao RNAi-4* (VDRC line 107645), *UAS-Tao RNAi-5* (TRiP line GL00015), *UAS-Hpo RNAi* (VDRC line 104169), *UAS-wts RNAi* (VDRC line 106174), *UAS yki RNAi* (VDRC line 104523), gbb^{1}*/CyO, act-GFP* (Wharton et al., 1999), wit^{A12}*/TM6B* (Marqués et al., 2002). Adult male *D. melanogaster* flies of various genotypes were crossed with female virgin *UAS-dcr2; D42-GAL4 or OK6-*GAL4 (neuronal expression), *or 24B-GAL4 or BG57-GAL4* (muscle expression) flies to drive either overexpression or loss of gene function by RNAi. With the exception of w^{1118}, gbb^{1}*/CyO, act-GFP, and* wit^{A12}*/TM6B*, all stocks crossed to the GAL4 lines contained an UAS element. After 2 days, the crosses were transferred onto fresh food daily. For Tao^{16} experiments, Tao^{16}*/FM7, dfd-YFP* virgin females were mated to w^{1118} males in embryo collection cages using yeasted grape juice plates which were changed daily. YFP-negative first instar larvae were transferred to fresh yeasted plates, and were sex selected 4 days later as wandering third instar larvae to distinguish Tao^{16} hemizygous males from Tao^{16}/w^{1118} heterozygous female control siblings. For the Tao^{16} rescue experiments, crosses were performed in embryo collection cages as described above. Tao^{16}*/FM7, actin-GFP; UAS-Tao/*

TM3, Ser, actin-GFP virgin females were mated to either *D42-GAL4* or *BG57-GAL4* males to drive neuronal or muscle Tao overexpression, respectively. GFP-negative first instar larvae were transferred to fresh yeasted plates, and were sex selected 4 days later as wandering third instar larvae to select Tao^{16} hemizygous males. All crosses were performed at 25°C.

NMJ dissection and Immunofluorescence

Larvae were grown at 25°C, and fillet or CNS dissections were prepared from wandering third-instar larvae. Briefly, the fillet dissections were performed in 1X PBS, by pinning the head and tail, and then cutting longitudinally along the dorsal midline and across the short-axis at A1 and A7. Innards were removed and cuticle was pinned down leaving only the body-wall musculature, which was then fixed in Bouin's fixative (Polysciences) for 10 minutes before being rinsed in 1X PBS. The fillet preparations were then transferred to PT (1X PBS + 0.1% Tx-100) in a microcentrifuge tube and were rinsed and blocked in PTN (1X PBS + 0.1% Tx-100 + 1% normal goat serum). Preparations that were later used for bouton quantification were then incubated in rabbit or goat anti-Horseradish Peroxidase (HRP) conjugated to a Cy3 or Alexa 488 fluorophore (Jackson Immunoresearch) at a 1:500 dilution and in either mouse anti-Discs large (Dlg) (4F3, DSHB) at a 1:500 dilution or mouse anti-Bruchpilot (Brp) (nc82, DSHB) at a 1:250 dilution in PTN overnight at 4°C; a donkey anti-mouse secondary antibody conjugated to Alexa 488 or Alexa 594 (Jackson Immunoresearch) was subsequently used at a 1:1000 dilution for 2–4 hrs at RT or overnight at 4°C to visualize Dlg or Brp. Other antibodies used include rabbit anti-Tao (Pflanz et al., 2015) at a 1:1000 dilution. Preparations were then rinsed in PTN and 1X PBS, prior to mounting in ProLong anti-fade mounting media (Invitrogen). CNS preparations followed a similar immunofluorescence staining protocol after dissection but were dissected in Schneider's media supplemented with 10% FBS (Sigma), and fixed in 4% paraformaldehyde (Polysciences) for 20 minutes before being transferred to borosilicate glass tubes for staining steps. Dissected CNSs were rinsed in 1X PBS before blocking for 1 hr in PTN at room temperature, as well as between primary and secondary antibodies, and after secondary antibody incubation. Antibodies used for CNS immunofluorescence included rabbit anti-pSMAD (1,5) (Cell Signaling 41D10) at a 1:100 dilution, rat anti-Elav (Elav-7E8A10, DSHB) at a 1:50 dilution, rabbit anti-Tao (Pflanz et al., 2015) at a 1:1000 dilution, and mouse anti-Repo (Repo-8D12, DSHB) at a 1:10 dilution in PTN overnight at 4°C. Donkey secondary antibodies conjugated to Alexa 488, Alexa 594, or Alexa 647 (Jackson Immunoresearch) were used at a 1:1000 dilution in PTN to visualize primary antibodies. CNSs were mounted in Invitrogen ProLong Gold anti-fade mounting media with DAPI (Invitrogen).

Imaging

Fillet dissection preparations and CNS preparations were imaged on a Zeiss LSM 800 laser scanning confocal microscope using a 40× or 100× objective.

Quantification of NMJ phenotypes

Boutons or Brp-positive puncta from muscle 4 of segments A2–4 of the fillet dissection preparations were counted using an Olympus BX60 epifluorescence microscope or a Zeiss Axioplan2 epifluorescence microscope using a 63× or 100× objective. For boutons from

NMJ 6/7, only segment A2 was scored. Muscle surface area was determined by imaging muscles from segments A2–4 of fillet dissections stained with Dlg using a 10× objective with a Zeiss Axioplan2 epifluorescence microscope. ImageJ was then used to measure the length and width of muscles, and surface area was calculated in Excel. NMJ length was determined by tracing the complete NMJ arbor of projected samples labeled with anti-HRP from at least 6 animals and representing at least 20 NMJ 4s using the NeuronJ plugin (ImageJ).

Electrophysiology

All recordings were performed as in (Menon et al., 2015). Briefly, age matched 3rd instar larvae were dissected in 0.3mM calcium HL3 saline (Stewart et al., 1994) (70mM NaCl, 5mM KCl, 20mM $MgCl_2$, 10mM $NaHCO_3$, 5mM Trehelose, 115mM Sucrose, 5mM HEPES). Body-wall muscles were visualized under a Nikon FS microscope using a 40× long-working distance objective and preparations were immersed in HL3 saline containing 0.5mM calcium. Recordings were performed by impaling muscle 6 in abdominal segments 3 and 4 with 15–20 MΩ sharp electrodes filled with 3M KCl. Signals were amplified using a MultiClamp 700B (Molecular Devices (MD)) and digitized using a Digidata 1550B (MD). Data was acquired using pClamp 10 software (MD) and analyzed using Mini Analysis software (Synaptosoft). Cut segmental nerves were drawn into a suction electrode and stimulated using a 1ms suprathreshold stimulus via a Master-9 stimulator (A.M.P.I.). Stimulation produced evoked excitatory junctional potentials (EJPs), while unstimulated preparations were recorded passively for miniature excitatory junctional potentials (mEJPs). Analysis was only performed on muscles cells with resting potentials below −60mV. Quantal content was calculated by dividing the mean EJP amplitude by the mean mEJP amplitude for each animal, and the resulting number pooled for each genotype.

pMad intensity quantification

Z-stacks of the ventral nerve cords of *Tao^{16}* and control heterozygotes, and *D42>Tao RNAi* and *D42/+* control animals were imaged on a Zeiss LSM 800 confocal at the same settings. From a single section representing the middle of the majority of midline motor neurons, the nuclei from ~2 commissures of each ventral nerve cord (VNC) (20 nuclei/animal) were circled as regions of interest and fluorescence intensity measured in both channels in ImageJ. A background circle was taken on each CNS in each channel and was subtracted from each measurement for that CNS before averaging the intensities. Dividing the intensity of pMad to that of Elav for the same nucleus produced a ratio of pMad:Elav intensity for each nucleus. These ratios were then average for each genotype. At least 8 animals of each genotype were examined.

qRT-PCR

Crosses to obtain *Tao^{16}* males and *Tao^{16}/w^{1118}* females were conducted as described above. Each genotype was dissected in Schneider's media supplemented with 10% FBS, to obtain 20–50 third instar CNSs. These were homogenized in a 1 mL dounce homogenizer using the RLT-plus buffer from a RNeasy plus kit (Qiagen). Further purification of total RNA followed the manufacturer's instructions. cDNA was synthesized using the iScript kit (Bio-Rad) and used between 115–250 ng total RNA (varied by experimental repeat but was

matched between samples). qRT-PCR was performed using custom-designed Taqman assays (Integrated DNA Technologies) in which the forward primer sequence spans an exon-exon junction. These were utilized in a StepOnePlus Real-Time PCR system (Applied Scientific/Thermo Scientific). *Rps17* was used as the reference gene for the delta delta Ct comparison protocol to quantify relative changes in gene expression, all in technical triplicate. No-reverse transcriptase controls were conducted to confirm the purity of each cDNA sample, and lack of gDNA contamination in the qRT-PCR. Four independent biological repeats were performed.

Data analysis

One-way ANOVA followed by Tukey's multiple comparison test or unpaired student's t-test were performed on raw data, while a Mann-Whitney test was performed on pMad:Elav ratios. All analyses were conducted in Prism 7 software (GraphPad) and differences were deemed statistically significant when $p<0.05$.

Results

Tao restricts NMJ growth independent of the Hippo pathway

The Hippo pathway is well-characterized as a tumor suppressor pathway in mitotic tissues. However, its role in restricting growth in post-mitotic tissues is less established. During larval development, epithelial tissues undergo tremendous growth that is sensitive to Hippo pathway signaling, raising the possibility that other tissues growing during the same developmental period may also be sensitive to the Hippo pathway. One such structure is the NMJ which must expand to keep pace with the drastic 100-fold increase in muscle surface area during larval growth (Gorczyca et al., 1993; Guan et al., 1996; Miller et al., 2012). Therefore, we investigated whether Hippo signaling could restrict proportional growth of motor neuron arbors during the larval development period.

In order to address the potential role of the Hippo pathway in larval NMJ growth, we used a targeted RNAi approach to knockdown individual components of the pathway (*Tao, hippo, warts,* and *yorkie*) in both motor neurons and in muscles. The RNAi lines in this study are well-characterized and reveal strong growth phenotypes in imaginal discs, comparable to somatic mosaic loss-of-function clones (Boggiano et al., 2011; Vissers et al., 2016). The GAL4/UAS system was used to express the RNAi pre- or postsynaptically (Brand & Perrimon, 1993). We found that knockdown of only one component of the core Hippo kinase cascade affected NMJ growth: presynaptic reduction of *Tao* lead to an increase in bouton numbers (Figure 1A–E, J). This defect is not due to expansion of the postsynaptic muscle since muscle size is unaltered (Supporting Information Figure S1A–B). The overgrowth observed due to loss of *Tao* is independent of the presynaptic GAL4 driver used, as OK6-GAL4, another motor neuron driver, elicits a similar overgrowth phenotype (Supporting Information Figure S1C). Although we scored muscle 4 NMJs due to ease of visualization and bouton counting, the overgrowth phenotype is independent of the NMJ studied, as the number of boutons on muscles 6/7 also increased (Supporting Information Figure S1D). Postsynaptic RNAi-mediated knockdown of *Tao*, and other Hippo pathway components, had no effect on synaptic growth or muscle size (Supporting Information Figure S1E–G),

suggesting that *Tao* function is required in motor neurons. The lack of phenotypes due to postsynaptic loss of *Tao* is also independent of the GAL4 driver, since using BG57-GAL4 (another muscle driver) results in wild-type bouton numbers (Supporting Information Figure S1H).

As a corollary to knockdown of Hippo pathway genes, we also overexpressed *Tao* and other components to determine if any may be rate-limiting for normal NMJ growth, since hyperactivity of Hippo pathway components in epithelial tissues leads to tissue undergrowth (Boggiano et al., 2011; Ho et al., 2010; Yu et al., 2010). Presynaptic overexpression of all Hippo pathway genes had no effect on NMJ development (Figure 1F–J). We tested two additional *Tao* overexpression lines as well as a version of *Tao* carrying a point mutation that renders the protein kinase-dead (Boggiano et al., 2011; Sato et al., 2007), and none showed significant changes in bouton numbers (Supporting Information Figure S1I), suggesting that while *Tao* is required for normal NMJ development, it may not be rate-limiting in the process.

To confirm that loss of *Tao* results in overgrown NMJs, we examined additional *Tao* RNAi transgenes. The presynaptic expression of four independent RNAi transgenes caused a statistically significant overgrowth of NMJ 4 without affecting muscle size (Supporting Information Figure S2A–I), similar to the initial RNAi line used. Furthermore, we utilized a hypomorphic allele of *Tao* that survives until the pupal stage, Tao^{16} (Pflanz et al., 2015), to complement the results from the RNAi transgenes. We observed a statistically significant increase in bouton number compared to heterozygous sibling controls (Figure 2A–C, F), confirming that *Tao* is required during NMJ development. Importantly, the Tao^{16} phenotype is rescued by expression of a *Tao* transgene in neurons (Figure 2D,F; Supporting Information Figure S2J–K). We were unable to rescue the phenotype with *Tao* expression in muscles (Figure 2E,F; Supporting Information Figure S2J–K). These data are consistent with the RNAi screen results showing that NMJ development was perturbed only by loss of *Tao* in neurons.

Tao expression in the larval nervous system has not been reported, though Tao activity is required in larval epithelial tissues (Boggiano et al., 2011; Poon et al., 2011). Utilizing a rabbit anti-Tao antibody, endogenous Tao is found in puncta in motor neuron boutons, supporting a role for presynaptic Tao in NMJ growth (Figure 2G). In Tao^{16} mutants, antibody staining was reduced at the NMJ (Figure 2H). Tao is also found in neuron and glial cell bodies in the VNC (Supporting Information Figure S2L,M). Surprisingly, Tao is also expressed in muscles (Figure 2G,H). However, knockdown of *Tao* expression in muscle does not seem to impact NMJ development (Supporting Information Figure S1E–H), and thus its role in muscles remains unknown.

Our data support a role for *Tao* that is independent of its conserved function in the Hippo pathway. Knockdown of *hippo* and *warts* had no effect on NMJ growth, despite Tao, Hippo, and Warts functioning together to inhibit Yorkie in epithelial growth. In order to provide further support for this model, we reasoned that knocking down *Tao* levels in combination with *yorkie* (*yki*), which on its own has no effect on NMJ development (Figure 1E, J), might suppress the *Tao*-dependent NMJ overgrowth. However, simultaneous loss of *Tao* and *yki* in

motor neurons shows the same phenotype as loss of *Tao* alone (Figure 3), without affecting muscle size (Supporting Information Figure S3). Together, these results suggest that Tao signals through a Hippo-independent pathway to exert its effect on NMJ development.

Characterization of *Tao* phenotypes

Each bouton contains several active zones that are responsible for the synaptic communication between the motor neuron and muscle. Given that Tao^{16} mutants have an increased number of boutons, we assessed if there was a corresponding increase in active zones. Bruchpilot (Brp) is an integral active zone protein, and Brp puncta serve as a proxy for active zone number (Barber et al., 2017; Liao et al., 2018; Wairkar et al., 2013). In Tao^{16} mutants, there are more active zones at NMJ 4 compared to control animals (Figure 4A–E; Tao^{16} mean = 335 puncta vs. Tao^{16}/w^{1118} mean = 272 puncta). However, the density of synaptic contacts appears consistent between control and Tao^{16} mutant animals (Figure 4F; Tao^{16} active zones per μm = 1.64 vs. Tao^{16}/w^{1118} active zones per μm = 1.78). Additional experiments comparing control animals to presynaptic knockdown of *Tao* show a similar density of Brp puncta (Supporting Information Figure S4A–F). This suggests that the supernumerary boutons in Tao^{16} mutants have normally spaced active zones.

To further characterize phenotypes seen when depleting neuronal *Tao*, we measured the length of each branch of NMJ 4 and summed the lengths of the individual branches to get a total NMJ 4 length value. *Tao* knockdown animals have an increase in overall branch length compared to wild-type controls without affecting muscle size (Supporting Information Figure S4G–H). Although *Tao* overexpression does not affect bouton development, we tested if *Tao* overexpression could decrease branch length, but found no change compared to controls (Supporting Information Figure S4G–H).

Tao mutations alter synaptic release

The increase in the total number of active zones upon knockdown of *Tao* suggests that NMJ function may also be altered. To address a role for *Tao* in NMJ physiology, we measured spontaneous and evoked activity in *Tao* mutants. Spontaneous events are calcium-independent, single quantal responses and have been implicated in the development of neural networks (reviewed in Andreae & Burrone, 2015). We recorded miniature excitatory junctional potentials (mEJPs) at muscle 6 and found no difference in either the amplitudes or frequencies between *Tao* mutants and heterozygous controls (Figure 5A–C). Next, we measured evoked excitatory junctional potentials (EJPs) which represent external stimulus driven, calcium-dependent activity, and found a substantial decrease in EJP amplitudes upon removal of *Tao* (Figure 5D–E). Since there was a decrease in EJP amplitude and no change in mEJP amplitude, quantal content was proportionately reduced (Figure 5F). Therefore, fewer synaptic vesicles (or quanta) are released with every evoked release event.

Tao negatively regulates the BMP pathway

NMJ development requires the well-characterized retrograde BMP pathway to promote synaptic growth. Since *Tao* functions independently of the Hippo pathway in NMJ growth, we examined if *Tao* had any role in BMP-mediated growth. In the canonical BMP pathway, the ligand, Gbb, is released by muscles and binds to the presynaptic type II BMP receptor

Wit. In heterozygous *gbb* or *wit* animals, the NMJs are comparable to wild-type controls and as discussed above, presynaptic knockdown of *Tao* leads to expansion of the NMJ. When the heterozygous BMP pathway mutants are introduced into the presynaptic *Tao* RNAi background, the supernumerary bouton phenotype is suppressed to wild-type or nearly wild-type levels (Figure 6A–G), without affecting muscle size (Supporting Information Figure S6), suggesting that *Tao* requires the BMP pathway to exert its effect on NMJ development.

We next examined if the BMP pathway is also required for the synaptic function defect observed in *Tao* mutants. Decrease in presynaptic *Tao* displayed normal spontaneous activity similar to *Tao* mutants, and removal of one copy of *gbb* in the neuronal *Tao RNAi* background had no effect (Figure 6H–J). Evoked activity was impaired upon reduction of presynaptic *Tao*, as in the *Tao* mutants, confirming that the defect in evoked activity is specific to the *Tao* locus (Figure 6K–L). Loss of one copy of *gbb* in the *Tao RNAi* background restored EJP amplitudes to normal levels (Figure 6K–L). Quantal content was also restored when removing one copy of *gbb* (Figure 6M), confirming that the BMP pathway is required for *Tao* control of synaptic function.

The novel interaction between the BMP pathway and *Tao* raises the question of whether *Tao* is acting upstream or downstream of the BMP pathway. If *Tao* is upstream, we hypothesized that manipulating *Tao* levels would affect BMP activity readouts, including phosphorylation of Mad and expression of BMP transcriptional targets. In agreement with this model, we observed a significant increase of nuclear phosphorylated Mad (pMad) in the larval VNC of Tao^{16} mutants compared to heterozygous siblings (Figure 7A–F), suggesting that *Tao* is a negative regulator of BMP activity. A similar increase in pMad was observed with neuronal knockdown of *Tao* (Supporting Information Figure S7). To further confirm that *Tao* acts upstream of BMP signaling, we performed qRT-PCR of *Cyp6a17*, a cytochrome P450 gene that is strongly downregulated in *wit* mutants (Kim & Marqués, 2010). In Tao^{16} mutants we observed a substantial upregulation of *Cyp6a17* (~8-fold) compared to heterozygous sibling controls (Figure 7G) consistent with a role for *Tao* as a repressor of the BMP pathway. Although we do not know how *Tao* regulates BMP signaling, this novel function for *Tao* may explain the supernumerary bouton phenotype in *Tao* loss-of-function.

Discussion

Tao functions independently of Hippo signaling

In this study, we sought to identify novel pathways that control larval NMJ development. We focused on the Hippo pathway due to its known function in regulating growth in various tissues. We tested several components of the Hippo pathway including the transcriptional co-activator Yorkie whose activity is regulated by three kinases (Tao, Hippo, and Warts). Surprisingly, only *Tao* is required for proper NMJ development. Upon knockdown of presynaptic *Tao*, the NMJ arbor expands, while the density of active zones is largely unchanged. Functionally, we found no change in spontaneous activity, although evoked responses were significantly reduced upon loss of *Tao*. Based on our finding that *Tao* does not require *yorkie* during NMJ development, we concluded that *Tao* functions independently of Hippo signaling to restrict NMJ growth. Instead, the dose-sensitive genetic interactions observed between *Tao* and components of the BMP pathway are indicative of genes that

function in the same genetic pathway and suggest that Tao requires BMP signaling during NMJ development and function. Additionally, we found that loss of *Tao* leads to elevated BMP signaling as evident by an increase in nuclear pMad and increased expression of *Cyp6a17,* a known BMP target gene, defining *Tao* as a new negative regulator of BMP signaling.

How does *Tao* affect NMJ development through BMP signaling?

Though our data posit *Tao* as a new inhibitor of BMP signaling, we do not yet know its mechanism of action. Two attractive possibilities include Tao negatively regulating BMP signaling at the level of BMP receptor membrane availability, or perhaps by directly regulating pMad levels. For example, the type I BMP receptor Thickveins (Tkv) is negatively regulated via phosphorylation by S6 Kinase-like (S6KL), which marks it for membrane removal and proteosomal degradation (Zhao et al., 2015). Increasing the membrane availability of Tkv in *S6KL* mutant animals increases BMP signaling, resulting in phenotypes reminiscent of *Tao* loss-of-function.

Alternatively, Tao could be a regulator of the downstream effector Mad. R-Smads are activated by C-terminal phosphorylation by the BMP type I receptors (Hoodless et al., 1996; Inoue et al., 1998). However, not all phosphorylations on Mad (or its mammalian homologs) are activating. Cyclin-dependent kinase 8 and Shaggy (GSK3 in mammals) are capable of phosphorylating R-Smads in a central linker domain, thereby promoting Smad degradation (Alarcón et al., 2009; Aleman et al., 2014). Drosophila Mad can also be regulated by Nemo phosphorylation at a distinct N-terminal residue (Merino et al., 2009; Zeng et al., 2007), possibly to regulate trafficking or nuclear localization of Mad. Perhaps more intriguing, Misshapen, a Ste20 family kinase (like Tao), and its mammalian homologs can phosphorylate Mad and inhibit its function at yet another distinct site (Kaneko et al., 2011). Of course, Tao might function in the BMP pathway via a different, undescribed mechanism.

An increase in synaptic outgrowth and neurotransmitter release sites, as observed with *Tao* knockdown, would suggest elevated synaptic vesicle release. However, single synapse analysis reveals that a majority of NMJ synapses are silent (Newman et al., 2017), thus an increase in active zones does not directly correlate to additional functional synapses. Interestingly, knockdown of specific genes that downregulate BMP signaling at the NMJ by promoting internalization of receptors show similar physiological properties as *Tao* mutants. For example, *spinster* mutations show a Tkv-dependent NMJ overgrowth phenotype, a decrease in evoked release, and no change in spontaneous amplitude (Sweeney & Davis, 2002). However, other mutations that upregulate BMP activity, such as in *S6KL*, show similar overgrowth defects, but no change in evoked release and instead an upregulation of spontaneous release amplitude, suggesting either changes in synaptic vesicle loading or changes in postsynaptic glutamate receptors (Zhao et al., 2015). The punctate localization of Tao at the periphery of boutons might suggest a role for Tao in regulating synaptic activity and BMP signaling through a *spinster*-dependent pathway and thus could be involved in the internalization of receptors.

Non-BMP dependent roles of *Tao*

NMJ development requires proper microtubule dynamics (Nechipurenko & Broihier, 2012) and cell adhesion molecules (reviewed in Menon et al., 2013), both of which are regulated by Tao in other contexts. Mammalian Tao (also known as MARKK) activates Par-1/MARK to inhibit microtubule stability, notably in neuronal cultures (Biernat et al., 2002; Timm et al., 2006). However, in adult *Drosophila* brains, Tao inhibits Par-1 and positively regulates the microtubule-stabilizing protein Tau during axon outgrowth and neurodegeneration (King et al., 2011; Wang et al., 2007), and there is also evidence that Tao-family kinases can directly phosphorylate Tau (Giacomini et al., 2018). Interestingly, BMP signaling also destabilizes microtubules via Spartin (Nahm et al., 2013). Thus, Tao may regulate microtubule stability through Spartin or Par-1 to affect NMJ development. Tao also negatively regulates cell surface levels of the neural cell adhesion molecule Fasciclin 2 (Fas2) (Gomez et al., 2012). Fas2 is required in NMJs for the proper formation of a synaptic terminal from an axon growth cone structure (Schuster et al., 1996), raising the possibility that Tao might also be acting to similarly regulate levels of Fas2 in developing NMJs.

Tao was recently implicated in *Drosophila* tracheal morphogenesis by its phosphorylation and activation of a related Ste20 kinase, GckIII (Poon et al., 2018). A role for GckIII in NMJ development has not been reported, but its mammalian homologs have been reported in a variety of axon outgrowth and synapse development processes (reviewed in Chen et al., 2018). In *Drosophila*, GckIII's target, the NDR-family kinase Tricornered (Trc), has been implicated in dendritic tiling (Emoto et al., 2006). If Tao functions through a GckIII-Trc signaling module in the NMJ this could provide further insight into how Tao regulates synaptic growth in a Hippo-independent manner. It is noteworthy that only three Tao substrates, Hippo, Par-1, and GckIII, have been identified. Further analysis of Tao in NMJ development may reveal novel substrates which can be further characterized in other Tao-dependent functions.

In summary, Tao plays a previously uncharacterized role in synaptic outgrowth, through negative regulation of BMP signaling. To our knowledge, this is the first report of a Tao kinase as a negative regulator of the BMP pathway, and it will be intriguing to see if Tao-family kinases can inhibit BMP signaling in other developmental contexts as well.

Supplementary Material

Refer to Web version on PubMed Central for supplementary material.

Acknowledgments

We wish to thank the Developmental Studies Hybridoma Bank, TRiP at the Harvard Medical School (NIH/NIGMS R01-GM084947), the Bloomington Stock Center (NIH P40OD018537), and Vienna Drosophila Resource Center for fly stocks and other reagents. We also wish to thank Heather Broihier, Colleen McLaughlin and the Broihier lab for training on NMJs and helpful discussions, Jeff Johansen for the use of his epifluorescence microscope, and Ralf Pflanz for the gift of the Tao16 mutant flies and anti-Tao antibody. Lastly, we want to thank John Carroll University for the funding to conduct this research. Research in R.A.C.'s lab was supported by National Institutes of Health Grant K01 NS102342.

References

Aberle H, Haghighi AP, Fetter RD, McCabe BD, Magalhães TR, & Goodman CS (2002). wishful thinking Encodes a BMP Type II Receptor that Regulates Synaptic Growth in Drosophila. Neuron, 33(4), 545–558. [PubMed: 11856529]

Alarcón C, Zaromytidou A-I, Xi Q, Gao S, Yu J, Fujisawa S, et al. (2009). Nuclear CDKs drive Smad transcriptional activation and turnover in BMP and TGF-beta pathways. Cell, 139(4), 757–769. [PubMed: 19914168]

Aleman A, Rios M, Juarez M, Lee D, Chen A, & Eivers E (2014). Mad linker phosphorylations control the intensity and range of the BMP-activity gradient in developing Drosophila tissues. Scientific Reports, 4, 6927. [PubMed: 25377173]

Andreae LC, & Burrone J (2015). Spontaneous Neurotransmitter Release Shapes Dendritic Arbors via Long-Range Activation of NMDA Receptors. Cell Reports.

Barber KR, Tanquary J, Bush K, Shaw A, Woodson M, Sherman M, & Wairkar YP (2017). Active zone proteins are transported via distinct mechanisms regulated by Par-1 kinase. PLoS Genetics, 13(2), e1006621. [PubMed: 28222093]

Biernat J, Wu Y-Z, Timm T, Zheng-Fischhöfer Q, Mandelkow E, Meijer L, & Mandelkow E-M (2002). Protein kinase MARK/PAR-1 is required for neurite outgrowth and establishment of neuronal polarity. Molecular Biology of the Cell, 13(11), 4013–4028. [PubMed: 12429843]

Boggiano JC, Vanderzalm PJ, & Fehon RG (2011). Tao-1 phosphorylates Hippo/MST kinases to regulate the Hippo-Salvador-Warts tumor suppressor pathway. Developmental Cell, 21(5), 888–895. [PubMed: 22075147]

Brand AH, & Perrimon N (1993). Targeted gene expression as a means of altering cell fates and generating dominant phenotypes. Development (Cambridge, England), 118(2), 401–415.

Budnik V, Koh YH, Guan B, Hartmann B, Hough C, Woods D, & Gorczyca M (1996). Regulation of synapse structure and function by the Drosophila tumor suppressor gene dlg. Neuron, 17(4), 627–640. [PubMed: 8893021]

Chen S, Fang Y, Xu S, Reis C, & Zhang J (2018). Mammalian Sterile20-like Kinases: Signalings and Roles in Central Nervous System. Aging and Disease, 9(3), 537–552. [PubMed: 29896440]

Collins CA, & DiAntonio A (2007). Synaptic development: insights from Drosophila. Current Opinion in Neurobiology, 17(1), 35–42. [PubMed: 17229568]

Deshpande M, & Rodal AA (2016). The Crossroads of Synaptic Growth Signaling, Membrane Traffic and Neurological Disease: Insights from Drosophila. Traffic (Copenhagen, Denmark), 17(2), 87–101.

Dong J, Feldmann G, Huang J, Wu S, Zhang N, Comerford SA, et al. (2007). Elucidation of a universal size-control mechanism in Drosophila and mammals. Cell, 130(6), 1120–1133. [PubMed: 17889654]

Emoto K, Parrish JZ, Jan LY, & Jan Y-N (2006). The tumour suppressor Hippo acts with the NDR kinases in dendritic tiling and maintenance. Nature, 443(7108), 210–213. [PubMed: 16906135]

Giacomini C, Koo C-Y, Yankova N, Tavares IA, Wray S, Noble W, et al. (2018). A new TAO kinase inhibitor reduces tau phosphorylation at sites associated with neurodegeneration in human tauopathies. Acta Neuropathologica Communications, 6(1), 37. [PubMed: 29730992]

Gomez JM, Wang Y, & Riechmann V (2012). Tao controls epithelial morphogenesis by promoting Fasciclin 2 endocytosis. The Journal of Cell Biology, 199(7), 1131–1143. [PubMed: 23266957]

Gorczyca M, Augart C, & Budnik V (1993). Insulin-like receptor and insulin-like peptide are localized at neuromuscular junctions in Drosophila. Journal of Neuroscience, 13(9), 3692–3704. [PubMed: 8366341]

Guan B, Hartmann B, Kho YH, Gorczyca M, & Budnik V (1996). The Drosophila tumor suppressor gene, dlg, is involved in structural plasticity at a glutamatergic synapse. Current Biology, 6(6), 695–706. [PubMed: 8793296]

Halder G, & Johnson RL (2011). Hippo signaling: growth control and beyond. Development (Cambridge, England), 138(1), 9–22.

Ho L-L, Wei X, Shimizu T, & Lai Z-C (2010). Mob as tumor suppressor is activated at the cell membrane to control tissue growth and organ size in Drosophila. Developmental Biology, 337(2), 274–283. [PubMed: 19913529]

Hoodless PA, Haerry T, Abdollah S, Stapleton M, O'Connor MB, Attisano L, & Wrana JL (1996). MADR1, a MAD-related protein that functions in BMP2 signaling pathways. Cell, 85(4), 489–500. [PubMed: 8653785]

Huang X, Shi L, Cao J, He F, Li R, Zhang Y, et al. (2014). The sterile 20-like kinase tao controls tissue homeostasis by regulating the hippo pathway in Drosophila adult midgut. Journal of Genetics and Genomics = Yi Chuan Xue Bao, 41(8), 429–438. [PubMed: 25160975]

Inoue H, Imamura T, Ishidou Y, Takase M, Udagawa Y, Oka Y, et al. (1998). Interplay of signal mediators of decapentaplegic (Dpp): molecular characterization of mothers against dpp, Medea, and daughters against dpp. Molecular Biology of the Cell, 9(8), 2145–2156. [PubMed: 9693372]

Jia J, Zhang W, Wang B, Trinko R, & Jiang J (2003). The Drosophila Ste20 family kinase dMST functions as a tumor suppressor by restricting cell proliferation and promoting apoptosis. Genes Dev, 17(20), 2514–2519. [PubMed: 14561774]

Jukam D, Xie B, Rister J, Terrell D, Charlton-Perkins M, Pistillo D, et al. (2013). Opposite Feedbacks in the Hippo Pathway for Growth Control and Neural Fate. Science (New York, NY), 342(6155), 1238016–1238016.

Kaneko S, Chen X, Lu P, Yao X, Wright TG, Rajurkar M, et al. (2011). Smad inhibition by the Ste20 kinase Misshapen. Pnas, 108(27), 11127–11132. [PubMed: 21690388]

Keshishian H, & Chiba A (1993). Neuromuscular development in Drosophila: insights from single neurons and single genes. Trends in Neurosciences, 16(7), 278–283. [PubMed: 7689772]

Keshishian H, Chiba A, Chang TN, Halfon MS, Harkins EW, Jarecki J, et al. (1993). Cellular mechanisms governing synaptic development in Drosophila melanogaster. Journal of Neurobiology, 24(6), 757–787. [PubMed: 8251016]

Kim NC, & Marqués G (2010). Identification of downstream targets of the bone morphogenetic protein pathway in the Drosophila nervous system. Developmental Dynamics : an Official Publication of the American Association of Anatomists, 239(9), 2413–2425. [PubMed: 20652954]

King I, Tsai LT-Y, Pflanz R, Voigt A, Lee S, Jäckle H, et al. (2011). Drosophila tao controls mushroom body development and ethanol-stimulated behavior through par-1. The Journal of Neuroscience : the Official Journal of the Society for Neuroscience, 31(3), 1139–1148. [PubMed: 21248138]

Koles K, & Budnik V (2012). Wnt signaling in neuromuscular junction development. Cold Spring Harbor Perspectives in Biology, 4(6), a008045. [PubMed: 22510459]

Liao EH, Gray L, Tsurudome K, El-Mounzer W, Elazzouzi F, Baim C, et al. (2018). Kinesin Khc-73/KIF13B modulates retrograde BMP signaling by influencing endosomal dynamics at the Drosophila neuromuscular junction. PLoS Genetics, 14(1), e1007184. [PubMed: 29373576]

Marqués G, Bao H, Haerry TE, Shimell MJ, Duchek P, Zhang B, & O'Connor MB (2002). The Drosophila BMP Type II Receptor Wishful Thinking Regulates Neuromuscular Synapse Morphology and Function. Neuron, 33(4), 529–543. [PubMed: 11856528]

McCabe BD, Hom S, Aberle H, Fetter RD, Marqués G, Haerry TE, et al. (2004). Highwire regulates presynaptic BMP signaling essential for synaptic growth. Neuron, 41(6), 891–905. [PubMed: 15046722]

McCabe BD, Marqués G, Haghighi AP, Fetter RD, Crotty ML, Haerry TE, et al. (2003). The BMP Homolog Gbb Provides a Retrograde Signal that Regulates Synaptic Growth at the Drosophila Neuromuscular Junction. Neuron, 39(2), 241–254. [PubMed: 12873382]

Menon KP, Carrillo RA, & Zinn K (2013). Development and plasticity of the Drosophila larval neuromuscular junction. Wiley Interdisciplinary Reviews: Developmental Biology, 2(5), 647–670. [PubMed: 24014452]

Menon KP, Carrillo RA, & Zinn K (2015). The translational regulator Cup controls NMJ presynaptic terminal morphology. Molecular and Cellular Neurosciences, 67, 126–136. [PubMed: 26102195]

Merino C, Penney J, González M, Tsurudome K, Moujahidine M, O'Connor MB, et al. (2009). Nemo kinase interacts with Mad to coordinate synaptic growth at the Drosophila neuromuscular junction. The Journal of Cell Biology, 185(4), 713–725. [PubMed: 19451277]

Miller DL, Ballard SL, & Ganetzky B (2012). Analysis of synaptic growth and function in Drosophila with an extended larval stage. The Journal of Neuroscience : the Official Journal of the Society for Neuroscience, 32(40), 13776–13786. [PubMed: 23035089]

Nahm M, Lee M-J, Parkinson W, Lee M, Kim H, Kim Y-J, et al. (2013). Spartin regulates synaptic growth and neuronal survival by inhibiting BMP-mediated microtubule stabilization. Neuron, 77(4), 680–695. [PubMed: 23439121]

Nechipurenko IV, & Broihier HT (2012). FoxO limits microtubule stability and is itself negatively regulated by microtubule disruption. The Journal of Cell Biology, 196(3), 345–362. [PubMed: 22312004]

Newman ZL, Hoagland A, Aghi K, Worden K, Levy SL, Son JH, et al. (2017). Input-Specific Plasticity and Homeostasis at the Drosophila Larval Neuromuscular Junction. Neuron, 93(6), 1388–1404.e10. [PubMed: 28285823]

Oh H, & Irvine KD (2011). Cooperative regulation of growth by Yorkie and Mad through bantam. Developmental Cell, 20(1), 109–122. [PubMed: 21238929]

Pflanz R, Voigt A, Yakulov T, & Jäckle H (2015). Drosophila gene tao-1 encodes proteins with and without a Ste20 kinase domain that affect cytoskeletal architecture and cell migration differently. Open Biology, 5(1), 140161. [PubMed: 25589578]

Poon CLC, Lin JI, Zhang X, & Harvey KF (2011). The Sterile 20-like Kinase Tao-1 Controls Tissue Growth by Regulating the Salvador-Warts-Hippo Pathway. Developmental Cell, 21(5), 896–906. [PubMed: 22075148]

Poon CLC, Liu W, Song Y, Gomez M, Kulaberoglu Y, Zhang X, et al. (2018). A Hippo-like Signaling Pathway Controls Tracheal Morphogenesis in Drosophila melanogaster. Developmental Cell, 47(5), 564–575.e5. [PubMed: 30458981]

Poon CLC, Mitchell KA, Kondo S, Cheng LY, & Harvey KF (2016). The Hippo Pathway Regulates Neuroblasts and Brain Size in Drosophila melanogaster. Current Biology : CB, 26(8), 1034–1042. [PubMed: 26996505]

Rawson JM, Lee M, Kennedy EL, & Selleck SB (2003). Drosophila neuromuscular synapse assembly and function require the TGF-beta type I receptor saxophone and the transcription factor Mad. Journal of Neurobiology, 55(2), 134–150. [PubMed: 12672013]

Ruiz-Canada C, & Budnik V (2006). Synaptic Cytoskeleton At The Neuromuscular Junction. International Review of Neurobiology, 75, 217–236. [PubMed: 17137930]

Sato K, Hayashi Y, Ninomiya Y, Shigenobu S, Arita K, Mukai M, & Kobayashi S (2007). Maternal Nanos represses hid/skl-dependent apoptosis to maintain the germ line in Drosophila embryos. Proceedings of the National Academy of Sciences of the United States of America, 104(18), 7455–7460. [PubMed: 17449640]

Schuster CM, Davis GW, Fetter RD, & Goodman CS (1996). Genetic dissection of structural and functional components of synaptic plasticity. I. Fasciclin II controls synaptic stabilization and growth. Neuron, 17(4), 641–654. [PubMed: 8893022]

Smith RB, Machamer JB, Kim NC, Hays TS, & Marqués G (2012). Relay of retrograde synaptogenic signals through axonal transport of BMP receptors. Journal of Cell Science, 125(Pt 16), 3752–3764. [PubMed: 22573823]

Stewart BA, Atwood HL, Renger JJ, Wang J, & Wu CF (1994). Improved stability of Drosophila larval neuromuscular preparations in haemolymph-like physiological solutions. Journal of Comparative Physiology. a, Sensory, Neural, and Behavioral Physiology, 175(2), 179–191.

Sweeney ST, & Davis GW (2002). Unrestricted synaptic growth in spinster-a late endosomal protein implicated in TGF-beta-mediated synaptic growth regulation. Neuron, 36(3), 403–416. [PubMed: 12408844]

Timm T, Matenia D, Li X-Y, Griesshaber B, & Mandelkow E-M (2006). Signaling from MARK to tau: regulation, cytoskeletal crosstalk, and pathological phosphorylation. Neuro-Degenerative Diseases, 3(4–5), 207–217. [PubMed: 17047359]

Varelas X, Sakuma R, Samavarchi-Tehrani P, Peerani R, Rao BM, Dembowy J, et al. (2008). TAZ controls Smad nucleocytoplasmic shuttling and regulates human embryonic stem-cell self-renewal. Nature Cell Biology, 10(7), 837–848. [PubMed: 18568018]

Wairkar YP, Trivedi D, Natarajan R, Barnes K, Dolores L, & Cho P (2013). CK2α regulates the transcription of BRP in Drosophila. Dev Biol, 384(1), 53–64. [PubMed: 24080510]

Wang J-W, Imai Y, & Lu B (2007). Activation of PAR-1 kinase and stimulation of tau phosphorylation by diverse signals require the tumor suppressor protein LKB1. The Journal of Neuroscience : the Official Journal of the Society for Neuroscience, 27(3), 574–581. [PubMed: 17234589]

Wharton KA, Cook JM, Torres-Schumann S, de Castro K, Borod E, & Phillips DA (1999). Genetic analysis of the bone morphogenetic protein-related gene, gbb, identifies multiple requirements during Drosophila development. Genetics, 152(2), 629–640. [PubMed: 10353905]

Wu S, Huang J, Dong J, & Pan D (2003). hippo encodes a Ste-20 family protein kinase that restricts cell proliferation and promotes apoptosis in conjunction with salvador and warts. Cell, 114(4), 445–456. [PubMed: 12941273]

Xu J, Vanderzalm PJ, Ludwig M, Su T, Tokamov SA, & Fehon RG (2018). Yorkie Functions at the Cell Cortex to Promote Myosin Activation in a Non-transcriptional Manner. Developmental Cell.

Yoshihara M, Rheuben MB, & Kidokoro Y (1997). Transition from growth cone to functional motor nerve terminal in Drosophila embryos. Journal of Neuroscience, 17(21), 8408–8426. [PubMed: 9334414]

Yu J, Zheng Y, Dong J, Klusza S, Deng W-M, & Pan D (2010). Kibra Functions as a Tumor Suppressor Protein that Regulates Hippo Signaling in Conjunction with Merlin and Expanded. Developmental Cell, 18(2), 288–299. [PubMed: 20159598]

Zeng YA, Rahnama M, Wang S, Sosu-Sedzorme W, & Verheyen EM (2007). Drosophila Nemo antagonizes BMP signaling by phosphorylation of Mad and inhibition of its nuclear accumulation. Development (Cambridge, England), 134(11), 2061–2071.

Zhao G, Wu Y, Du L, Li W, Xiong Y, Yao A, et al. (2015). Drosophila S6 Kinase like inhibits neuromuscular junction growth by downregulating the BMP receptor thickveins. PLoS Genetics, 11(3), e1004984. [PubMed: 25748449]

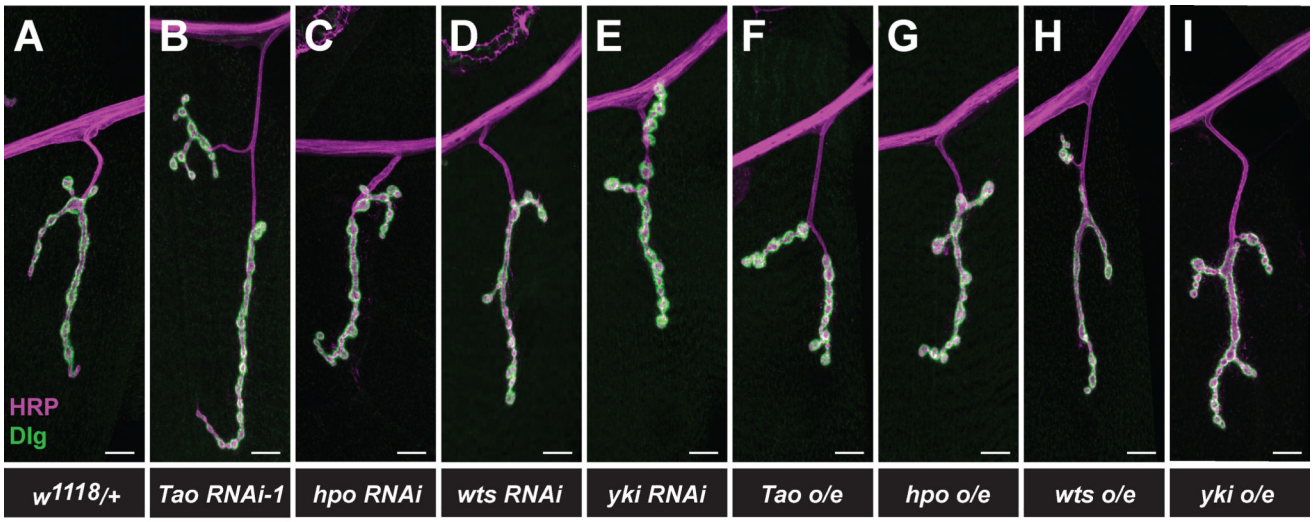

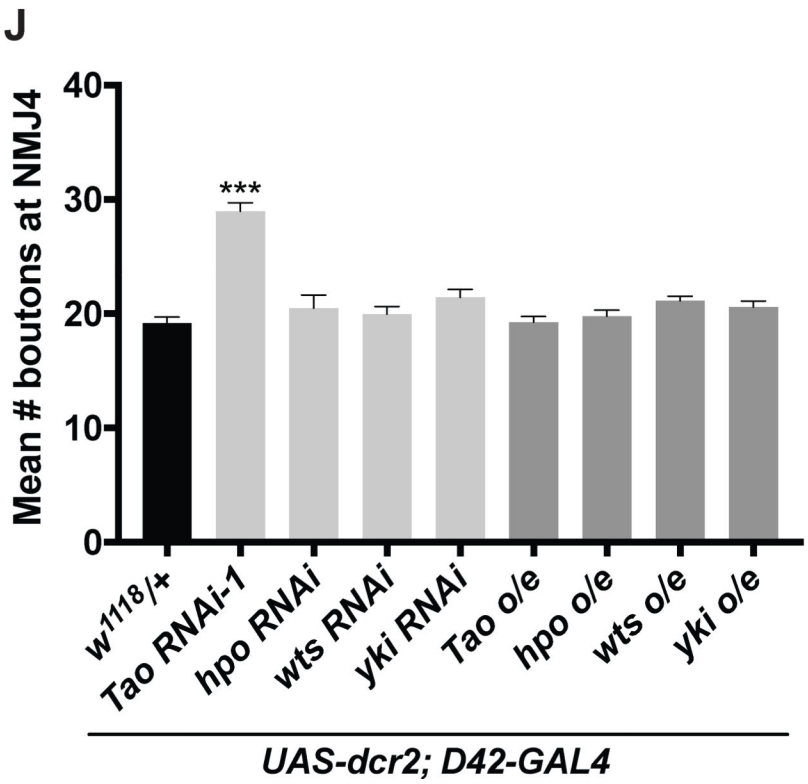

Figure 1. *Tao*, but not other Hippo pathway components, is required presynaptically for normal NMJ development.

(**A-I**) Merged representative maximum projections of NMJ 4 stained with HRP (magenta) and Dlg (green) to show the neuronal membrane and subsynaptic reticulum, respectively, from each genotype.

(**J**) Loss of presynaptic *Tao,* but not other core Hippo pathway components, using the D42 motor neuron GAL4 driver (light gray bars), significantly increases bouton number. n = 82, 79, 41, 51, and 70, respectively. Overexpression of Hippo pathway components presynaptically using the *D42-GAL4* driver (dark gray bars) does not affect NMJ

development. n= 52, 89, 86, and 46, respectively. Error bars show SEM, ***$p<0.0001$, Scale bar represents 10 μm. See also Supplemental Information Figure S1.

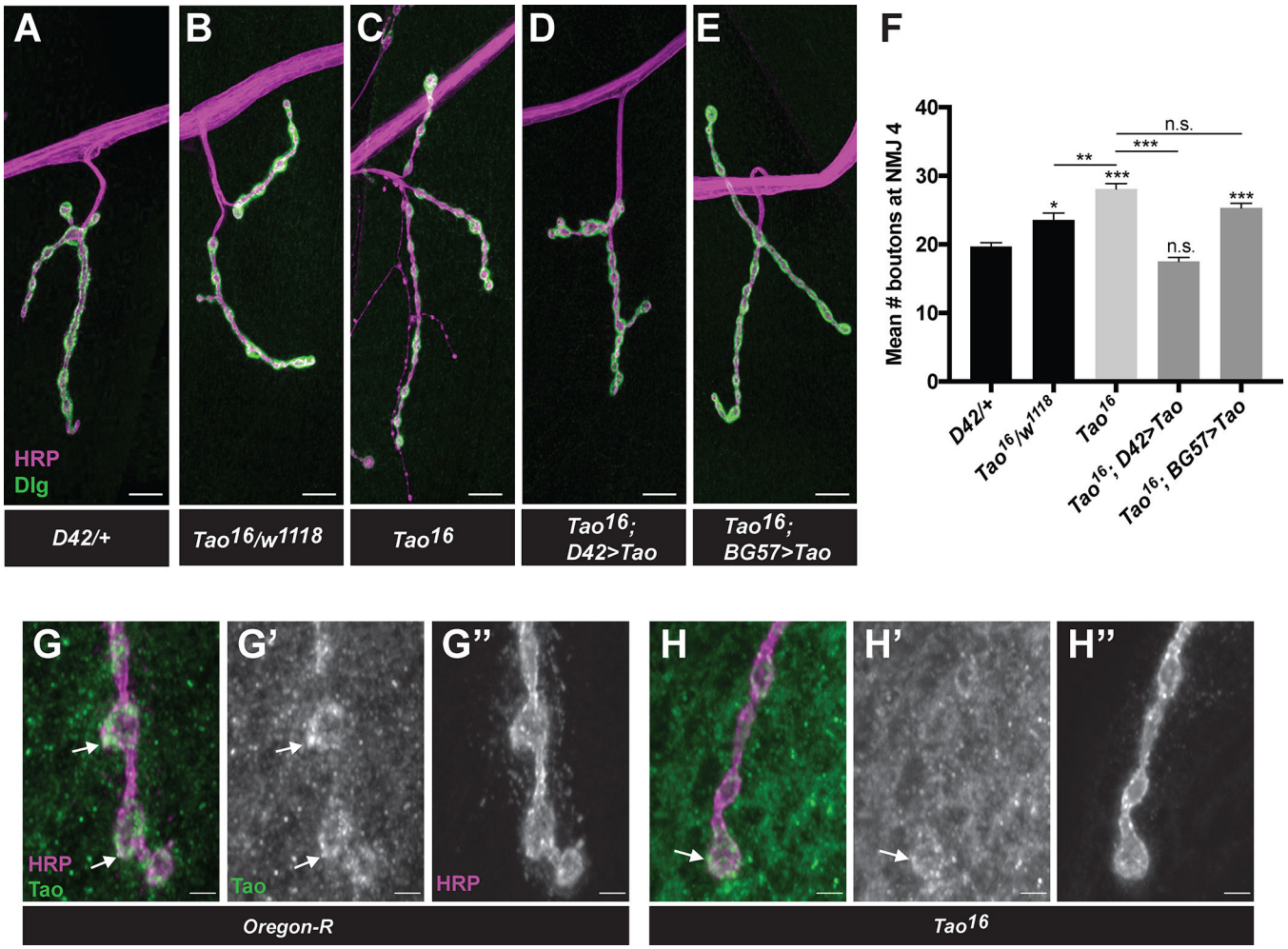

Figure 2. *Tao* controls NMJ development presynaptically and is expressed in NMJs.

(**A**-**F**) Merged representative maximum projections of NMJ 4 stained with HRP (magenta) and Dlg (green) of the genotypes depicted in (**F**). (**A**-**C**,**F**) A *Tao* hypomorph (*Tao*^{16}) had more boutons at NMJ 4 compared to controls. (**D**-**F**) *Tao*^{16} bouton phenotype is rescued by neuronal (**D**,**F**), not muscle (**E**,**F**) expression of *Tao*. For (**F**), n = 41, 41, 75, 82, and 44, respectively.

(**G**,**H**) Endogenous Tao expression at NMJ 4. (**G**) Merged representative maximum projections of the distal portion of NMJ 4 stained with HRP (magenta) and Tao (green) in control animals. Arrows highlight puncta of Tao and HRP colocalization. (**H**) There is decreased Tao staining in *Tao*^{16} mutants (images in (**G**,**H**) were taken at the same settings). Arrows point to boutons with residual faint Tao colocalizing with HRP. Error bars show SEM, **p*<0.05, ***p*<0.01, ****p*<0.0001, n.s. = not significant. Scale bar represents 10 μm in (**A**-**E**) and 2 μm in (**G**,**H**). See also Supplemental Information Figure S2.

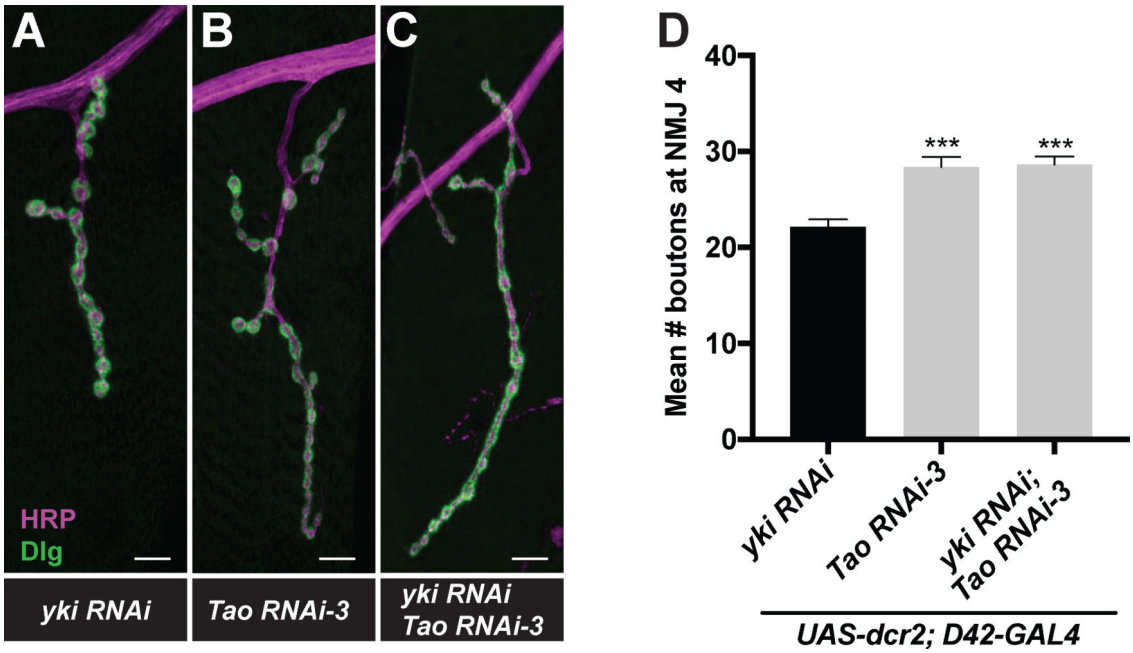

Figure 3. *Tao* functions in NMJ development independent of the Hippo pathway.

(**A**-**C**) RNAi-mediated knockdown of *Tao* and *yki* was performed presynaptically. Merged representative maximum projections of NMJ 4 stained with HRP (magenta) and Dlg (green). (**D**) Loss of *Tao* resulted in increased bouton numbers, even in the absence of *yki* function. N = 46, 37, and 28, respectively in (**D**). Error bars show SEM, ****p<0.0001*. Scale bar represents 10 μm in (**A**-**C**). See also Supplemental Information Figure S3.

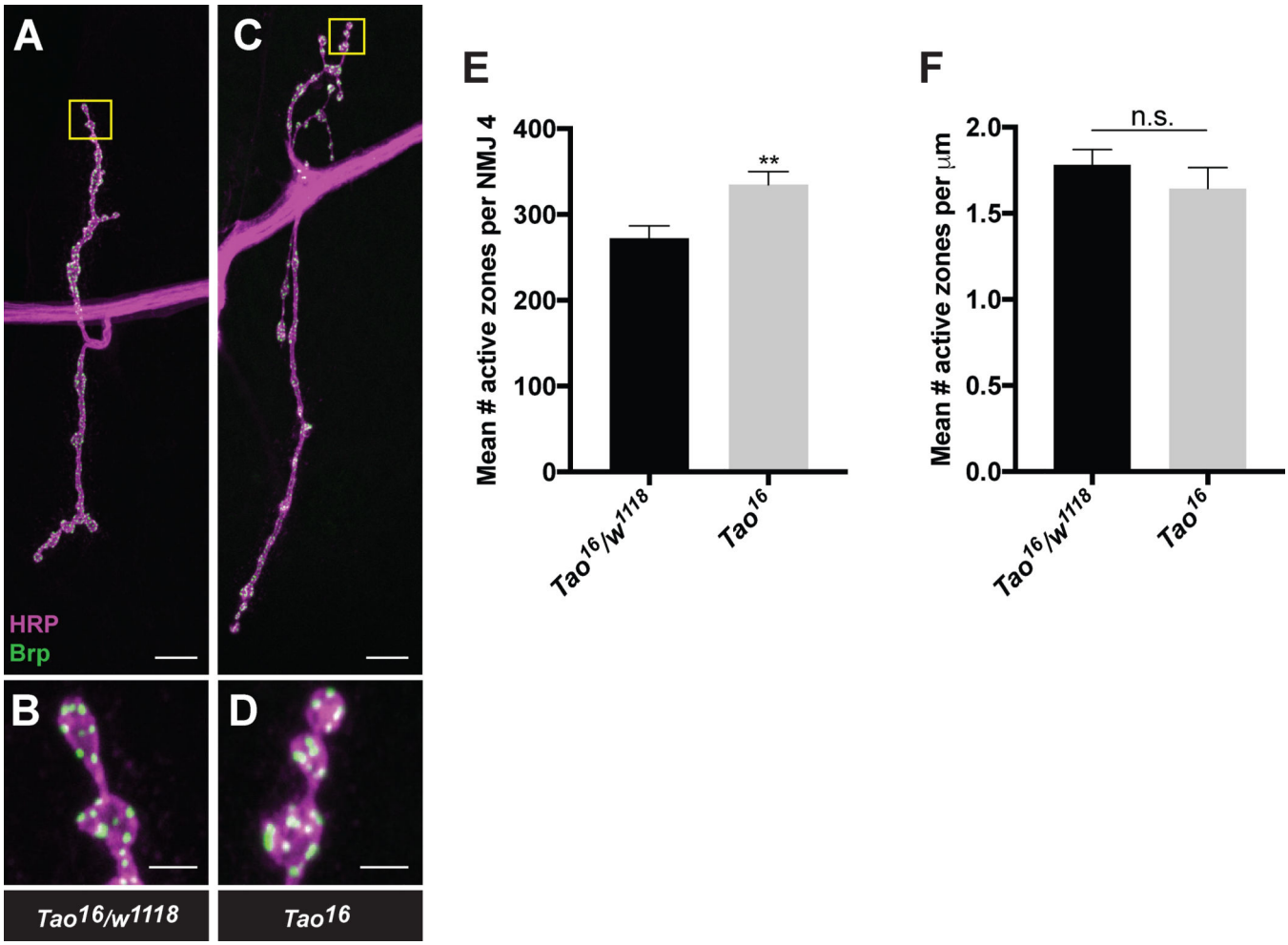

Figure 4. NMJs lacking *Tao* have an increased number of active zones.

(**A-D**) Merged representative maximum projections of NMJ 4 stained with HRP (magenta) and Brp (green) of control and Tao^{16} mutant animals. The yellow boxed area is enlarged in (**B,D**) for each image shown in (**A,C**).

(**E**,**F**) Quantification of Brp-positive active zones. NMJs lacking *Tao* have an increased number of active zones while the density of active zones (boutons per total NMJ length) is unchanged. n = 21, and 20, respectively in (**E**) and (**F**). Error bars show SEM, ***p<0.01,* n.s. = not significant. Scale bar represents 10 µm in (**A**,**C**) and 2 µm in (**B,D**). See also Supplemental Information Figure S4.

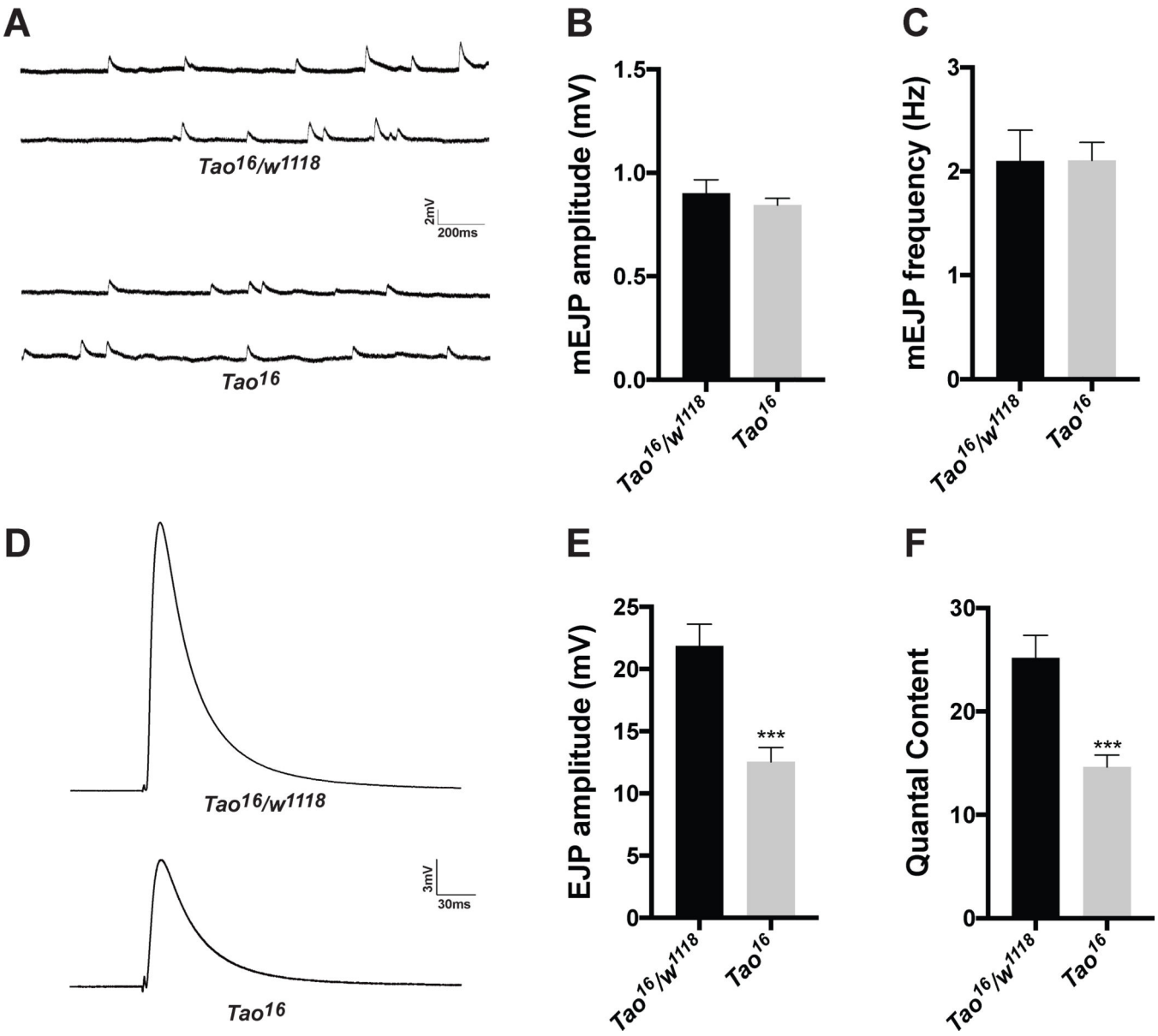

Figure 5. *Tao* mutants impact synaptic release.

(**A**) Representative traces of spontaneous events in heterozygous controls and *Tao* hypomorphs.

(**B**,**C**) Quantification of spontaneous activity, showing no significant change in either (**B**) spontaneous amplitude or (**C**) frequency.

(**D**) Representative traces of evoked events in the respective genotypes.

(**E**,**F**) Mutant animals show a drastic reduction in (**E**) EJP amplitude, and by extension (**F**) quantal content. n = (animals/muscles) 5/11, 7/14 respectively. Error bars show SEM, ***$p<0.0001$.

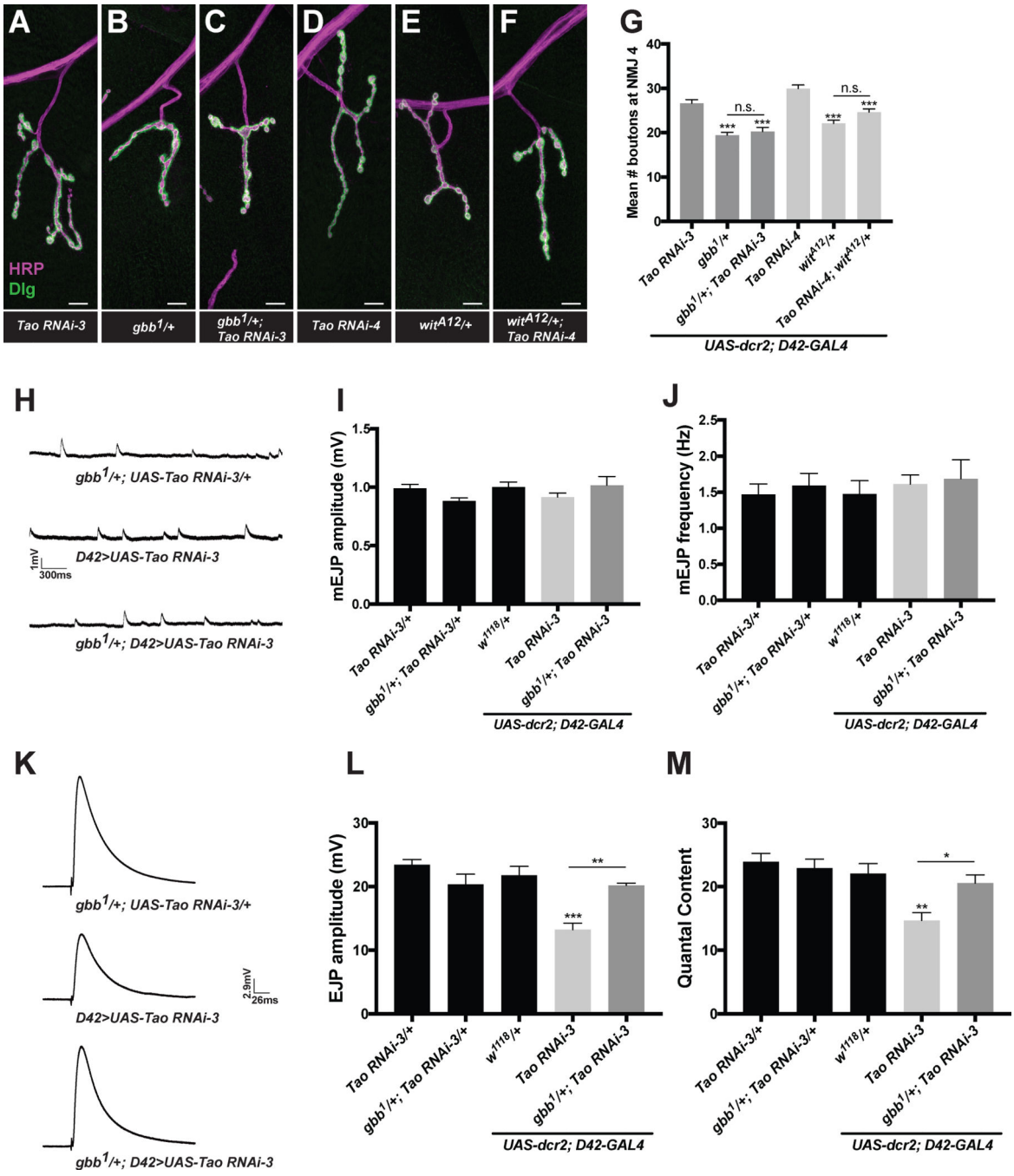

Figure 6. *Tao* requires BMP signaling to affect NMJ development and function.

(**A**-**F**) Merged representative maximum projections of NMJ 4 stained with HRP (magenta) and Dlg (green) from each genotype.

(**G**) Quantification of bouton number in respective genotypes. n = 47, 42, 37, 37, 33, and 38, respectively.

(**H**) Representative traces of spontaneous events in respective genotypes.

(**I**,**J**) Quantification of spontaneous activity, showing no significant change in either (**I**) amplitude or (**J**) frequency.

(**K**) Representative traces of evoked events in the respective genotypes.
(**L**,**M**) Knockdown of *Tao* in motor neurons shows a drastic reduction in (**L**) EJP amplitude and (**M**) quantal content. n = (animals/muscles) 7/12, 5/12, 7/10, 10/22, 6/9 respectively. Error bars show SEM, *$p<0.05$, **$p<0.01$, ***$p<0.0001$, n.s. = not significant. Scale bars represent 10 μm in (**A**-**F**). See also Supplemental Information Figure S6.

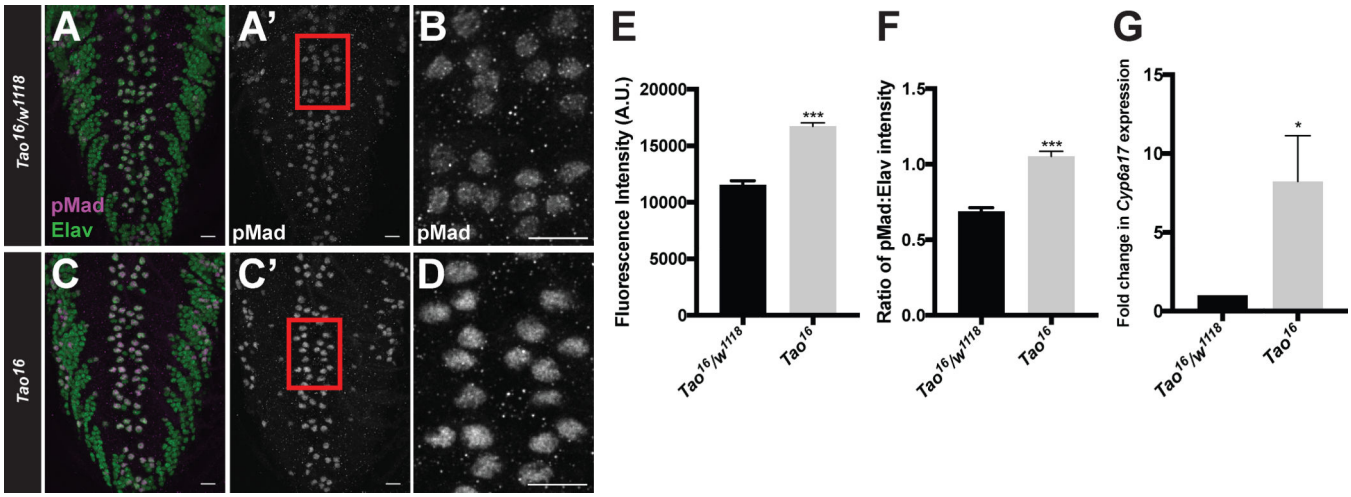

Figure 7. *Tao* negatively regulates BMP signaling.

(**A**-**D**) Representative merged maximum intensity projections of VNC neurons from control and *Tao*^{16} animals, stained for Elav and pMad. (**B**, **D**) are enlargements of the boxed areas in (**A'**) and (**C'**), respectively. (**A'**,**C'**) are the pMad channel from the merged images in (**A**) and (**C**), respectively.

(**E**,**F**) Quantification of fluorescence intensity from single z-sections showed a statistically significant increase in pMad intensity in motor neurons (**E**) and an increase in the ratio of pMad to Elav (**F**) in *Tao*^{16} compared to sibling controls.

(**G**) qRT-PCR from 3rd instar larval CNS for *Cyp6a17*, a known target gene of BMP signaling showed a statistically significant increase in expression in *Tao*^{16} compared to controls (average of 4 independent experiments depicted), Error bars show SEM, $*p<0.05$, $***p<0.0001$. Scale bars represent 10 μm in (**A**-**D**). See also Supplemental Information Figure S7.